

Parsec-scale radio structures in the nuclei of four Seyfert galaxies

Marek J. Kukula

Space Telescope Science Institute, 3700 San Martin Drive, Baltimore, MD 21218, U.S.A. and
Institute for Astronomy, University of Edinburgh, Royal Observatory, Blackford Hill, Edinburgh
EH9 3HJ, U.K., kukula@stsci.edu

Tapasi Ghosh

Arecibo Observatory, P.O. Box 995, Arecibo, Puerto Rico, PR 00613, U.S.A., tghosh@naic.edu

Alan Pedlar

NRAL, University of Manchester, Jodrell Bank, Macclesfield SK11 9DL, U.K., ap@jb.man.ac.uk

and

Richard T. Schilizzi

Joint Institute for VLBI in Europe, P.O. Box 2, 7990 AA, Dwingeloo, the Netherlands and Leiden
Observatory, P.O. Box 9513, 2300 RA Leiden, the Netherlands, rts@nfra.nl

ABSTRACT

We present 18-cm radio maps of four Seyfert nuclei, Mrk 1, Mrk 3, Mrk 231 and Mrk 463E, made with the European VLBI Network (EVN). Linear radio structures are present in three out of four sources on scales of ~ 100 pc to ~ 1 kpc, and the 20-mas beam of the EVN enables us to resolve details within the radio structures on scales of < 10 pc. Mrk 3 was also imaged using MERLIN and the data combined with the EVN data to improve the sensitivity to extended emission. We find an unresolved flat-spectrum core in Mrk 3, which we identify with the hidden Seyfert 1 nucleus in this object, and we also see marked differences between the two highly-collimated radio jets emanating from the core. The western jet terminates in a bright hotspot and resembles an FR II radio structure, whilst the eastern jet has more in common with an FR I source. In Mrk 463E, we use the radio and optical structure of the source to argue that the true nucleus lies approximately 1 arcsec south of the position of the radio and optical brightness peaks, which probably represent a hotspot at the working surface of a radio jet. The EVN data also provide new evidence for a 100-pc radio jet powering the radio source in the Type 1 nucleus of Mrk 231. However, the Seyfert 2 galaxy Mrk 1 shows no evidence for radio jets down to the limits of resolution (~ 10 pc). We discuss the range of radio source size and morphology which can occur in the nuclei of Seyfert galaxies and the implications for Seyfert unification schemes and for radio surveys of large samples of objects.

Subject headings: galaxies: active — galaxies: individual (Mrk 1, Mrk 3, Mrk 231, Mrk 463) — galaxies: jets — galaxies: Seyfert — radio continuum: galaxies

1. Introduction

Seyfert galaxies are the nearest and most numerous class of active galaxy and, although they are radio-weak, the nuclei of many Seyferts contain compact non-thermal radio sources which often account for a large fraction of the total radio luminosity of the galaxy. Aperture synthesis with instruments such as the VLA and MERLIN has resolved these radio sources, in many cases revealing linear, highly-collimated structures (*eg* Ulvestad & Wilson 1984a,b, Pedlar et al. 1993) and there is now little doubt that at least some Seyfert galaxies are capable of producing radio jets which are qualitatively similar to those found in radio-loud quasars and radio galaxies, albeit several orders of magnitude smaller and less powerful.

Because of their proximity, Seyfert nuclei present us with the opportunity to study jet structure on the smallest possible spatial scales, with a level of detail which is impossible for more luminous, but also more distant, quasars and radio galaxies. In this paper we report on very long baseline interferometer (VLBI) observations of four Markarian Seyfert galaxies, Mrk 1, Mrk 3, Mrk 231 and Mrk 463E (see Table 1). Preliminary results of this project were presented by Ghosh et al. (1994).

We assume $H_0 = 75 \text{ kms}^{-1}\text{Mpc}^{-1}$ throughout this paper. The spectral index, α , is defined according to the relation $S \propto \nu^\alpha$, where S is the flux density at frequency ν .

1.1. Radio emission and the standard model of Seyfert nuclei

Several studies have attempted to use radio observations of large samples of objects to test models of Seyfert activity. In particular, the radio properties are regarded as ideal for testing schemes which attempt to unify Seyfert 1s and 2s via viewing angle effects. According to this scenario all Seyfert nuclei are surrounded by an optically thick torus which lies in the plane perpendicular to the axis of the radio jets. When our line of sight to the nucleus intersects the torus, the central engine and broad line region (BLR) are blocked from view and we classify the object as a Seyfert 2. If our view of the nucleus is unobstructed, we call the object a Seyfert 1. Assuming that the radio emission is isotropic and unaffected by dust obscuration, the model predicts that the average radio luminosities of Types 1 and 2 should be the same and also that the radio jets in Seyfert 1s should be foreshortened on average relative to those in Seyfert 2s due to projection effects.

To date, radio surveys of Seyferts have produced conflicting results, some of which can be ascribed to selection effects in the samples themselves (*eg* due to the greater difficulty in identifying Seyfert 2s; on average those that are detected tend to be more luminous than Seyfert 1s). However, even when such effects have been removed, or compensated for as far as is possible, confusion still remains. Kukula et al. (1995) found that the radio structures of Seyfert 1s in the CfA sample (Huchra & Burg 1992) were on average too compact to be foreshortened versions

of the Type 2 objects in the same sample, indicating that orientation is not the only effect at work in this particular case. Indeed, only 1/26 Seyfert 1s in the CfA sample showed any sign of extended radio structure down to the $0.24''$ resolution of the VLA. Meanwhile, Roy et al. (1994), in a single-baseline VLBI study of several Seyfert samples, found that Type 1 objects were *less* likely than Type 2s to contain compact nuclear radio components, contrary to what would be expected from the simple unified model. Finally, Thean et al. (1998) report that Seyfert 1s and 2s in the Extended $12\mu\text{m}$ AGN Sample (Rush, Malkan & Spinoglio 1993) are *equally likely* to contain extended radio sources, with no significant difference between the size distributions of the two types.

In practice the effects of the various selection criteria and observational biases operating in these samples are very difficult to quantify without a better understanding of the physical processes which are responsible for the radio emission. Detailed studies of individual Seyferts offer perhaps the best means of achieving this goal, and VLBI - though an inefficient tool for large surveys - is ideally suited to this kind of work.

1.2. VLBI observations of Seyfert nuclei

VLBI provides the highest angular resolution of any imaging technique but in the past sensitivity constraints were extremely tight, effectively limiting VLBI studies of active galaxies to the small fraction of objects which are radio loud. However, technological advances made over the last decade have resulted in large increases in sensitivity, and imaging of the brightest radio-quiet objects is now well within the capability of modern instruments.

Several recent VLBI studies of Seyfert nuclei have provided detailed images of structures close to the central engine itself (eg Halkides, Ulvestad & Roy 1997; Mundell et al. 1997; Oosterloo et al. 1998; Ulvestad, Wrobel & Carilli 1998; Roy et al. 1998). Often the radio structure on milliarcsecond (parsec) scales is misaligned with the large-scale (~ 100 pc) radio jets familiar from low-resolution maps. These discoveries pose challenges for traditional unified models of Seyferts because they imply that the aligned arcsecond-scale radio continuum and optical line emission cannot necessarily be used to trace the symmetry axis of the central engine.

However, in some cases the physical properties of the VLBI radio source suggest an entirely different origin to the emission on larger scales. In the nucleus of NGC 1068, the archetypal Seyfert 2 galaxy, Gallimore, Baum & O’Dea (1997) found a linear radio structure ~ 1 pc across, lying almost perpendicular to the arcsecond-scale synchrotron jet. They suggest that this feature represents free-free emission from the inner edge of a molecular torus surrounding the AGN - the first direct observational evidence for such a structure. Ulvestad, Roy, Colbert & Wilson (1998), consider a similar explanation for the misaligned sub-parsec radio structure in NGC 4151.

2. Observations and data reduction

Observations were made in Autumn 1990 (see Table 1 for dates) with the European VLBI Network (EVN), a radio interferometer spanning Western Europe and at this time incorporating telescopes in Germany (Effelsberg), Sweden (Onsala), Italy (Medicina) and the U.K. (Jodrell Bank). The observing frequency was 1655 MHz (18 cm), giving an angular resolution in the final maps of ~ 20 mas - a factor of 2.5 higher than that of the restored Hubble Space Telescope. The data recording was in MKIII mode B with a bandwidth of 28 MHz. Two calibration sources, OQ208 and DA193, were interleaved with the four target sources during the 4 days of the observing run, with approximately 10 hours spent on each target source. The amplitude calibration was carried out using the system temperatures measured before and after each 13-minute scan and the gain curves supplied by each station. Global fringe-fitting was performed on the calibration sources using point source models, and the resulting single-band and multi-band delays were interpolated to the entire data-set. The data for each source were then fringe-fitted again and delays and rates were adjusted before frequency and time averaging were performed. For Mrk 3, the previously made 18-cm MERLIN map (see below) was used for the model, both for global fringe fitting and for the first round of self calibration. For the other three sources, point source models were used and hence the absolute position information has not been retained. The calibration sources were also processed through several cycles of phase-self-calibration and mapping. The resulting flux densities for the two sources at this epoch of observation were $S_{OQ208} = 0.8$ Jy and $S_{DA193} = 1.8$ Jy. We estimate an uncertainty of $\sim 10\%$ in the flux densities. For the final maps, a uniform weighting scheme was used for the Fourier transform in order to maximize the angular resolution. The RMS noise levels were typically 0.15 - 0.2 mJy.

Eight hours of additional 18-cm (1658 MHz) observations were made of one object, Mrk 3, on April 26th 1993 with the Multi-Element Radio Linked Interferometer Network (MERLIN), operated from Jodrell Bank. The MERLIN and EVN data were calibrated separately and the visibilities then combined, with appropriate weighting, to give a single large dataset. The MERLIN data helps to fill the ‘hole’ in the center of the uv plane caused by the EVN’s lack of short baselines. After the Fourier transform and deconvolution, the resulting map retained both the high angular resolution of the EVN and MERLIN’s greater sensitivity to extended radio emission.

3. Results

Compact radio components were detected in all four Seyferts, with three objects displaying prominent linear radio structures. The measured positions, flux densities, sizes and various derived properties of the individual radio components are given in Table 2 (Mrk 1, 231 & 463) and Table 3 (Mrk 3). Flux densities and positions were measured from the maps using the AIPS task TVSTAT. Deconvolved angular sizes for the components were obtained from two-dimensional Gaussian fits to the data using the task JMFIT or, for the more irregular features, were estimated from the maps.

Estimates of the magnetic field density in the radio-emitting regions derived from minimum energy arguments (*eg* Miley 1980), give typical values of $\sim 10^{-7}\text{T}$ (Tables 2 & 3). The corresponding lifetime for synchrotron-emitting electrons in a field of this strength is $\sim 10^4$ years. Brightness temperatures, T_B , of the compact radio features are typically 10^{6-7}K , similar to the values measured in other Seyfert nuclei with the VLBA (Gallimore et al. 1997; Ulvestad et al. 1998; Carilli et al. 1998). However, the spatial resolution of the current maps is insufficient to determine whether parsec- or subparsec-scale free-free emission from a molecular torus might be present in any of the objects in our sample.

3.1. Markarian 1

This Seyfert 2 galaxy is perhaps best known for the prominent water maser in its nucleus (Braatz, Wilson & Henkel 1994). Keel (1996) suggests that the galaxy is interacting with the nearby object NGC 451. No evidence for broad lines - indicative of a ‘hidden’ Seyfert 1 nucleus - has been found in Mrk 1, either in polarized light (Kay 1994) or in the infrared (Veilleux, Goodrich & Hill 1997).

Mulchaey & Wilson (1995) report that the $[\text{OIII}]\lambda 5007$ emission in Mrk 1 is extended along PA83°, whilst Ulvestad, Wilson & Sramek (1981), using the VLA at 6 cm, found the radio structure to consist of a barely resolved nuclear source with weaker emission extending ~ 400 mas (~ 120 pc) to the south.

In the EVN map (Figure 1) we find a compact radio core (deconvolved size ~ 10 mas = 3 pc) surrounded by a halo of emission approximately 100 mas (~ 30 pc) across. This extended emission appears to be elongated in approximately the same direction as the optical emission line region, although we note that the restoring beam also has a similar orientation. There is also some evidence for weak emission extending to the south, perhaps leading into the larger structure reported by Ulvestad, Wilson & Sramek. We find no evidence for linear radio structure in this object on any scale larger than a few parsecs.

3.2. Markarian 3

Mrk 3 is an early-type (S0 or elliptical) galaxy with a Seyfert 2 nucleus, although the presence of broad emission lines in its polarized spectrum argues strongly for a hidden Seyfert 1 nucleus in this object (Schmidt & Miller 1985; Miller & Goodrich 1990, Tran 1995), as does the photon budget calculated by Capetti et al. (1995a). It is the nearest object in the current study; at a distance of only 55 Mpc we obtain a spatial resolution of 5 pc with the EVN. In an earlier study of this object with MERLIN at 6 cm, we found a highly-collimated ‘S’-shaped radio structure with a bright radio ‘hotspot’ at its western end (Kukula et al. 1993). HST imaging of the Narrow Line Region shows that the jet is surrounded by a sheath of line-emitting gas (Capetti et al. 1995a),

but there is no direct one-to-one correspondence between the individual radio components and brightness peaks in the line emission.

By concatenating 18-cm data from the EVN and MERLIN, with suitable weighting of the data, we retain both the high angular resolution of the former and the sensitivity to more extended emission provided by the shorter baselines of the latter. The result, shown in Figure 2, reveals a wealth of detail, with both the jets and the western hotspot containing complicated substructure. In Figure 2, we adopt the same naming scheme for the radio components as used to describe our 6-cm MERLIN map, with the addition of component 1a, at the eastern end of the structure (which was only marginally detected in the MERLIN map), and with the refinement of letters to denote the most prominent small-scale features.

The jets consist of a string of compact knots encased in a streamer of more diffuse emission with a marked ‘S’-shaped curvature. There appears to be no systematic increase or decrease in the brightness of the knots along the length of the jet. The jet is resolved in the transverse direction and its width is fairly constant (~ 100 mas) along its length. However there are several regions in which there appears to be little or no radio emission: between the weak, diffuse components 1a & 1; on either side of the unresolved component 4; and between the jet and the bright western ‘hotspot’.

3.2.1. *Spectral index variations along the jet*

In order to study the variation in spectral index across the radio source we convolved our 18-cm EVN map with a $0.09'' \times 0.07''$ beam to make it directly comparable to our previous 6-cm MERLIN map (Kukula et al. 1993). Using the AIPS task COMB to compare the two datasets resulted in the spectral index map reproduced in Figure 3. Spectral indices for the individual components are listed in Table 3.

The map shows the jet to have a steep spectrum, with a typical spectral index of $\alpha \sim -1$. The compact features generally have a slightly flatter spectrum than the diffuse emission, although the only knot with a genuinely flat spectrum is the unresolved component 4.

The proximity of component 4 to the peak of the optical continuum emission (as measured by Clements 1981), and its position at the center of symmetry of the ‘S’, first led us to suggest that it might be the radio core of Mrk 3 (Kukula et al. 1993). The newly-derived flat spectrum for this component supports this view since it is characteristic of synchrotron self-absorption (SSA), a property which is often observed in the core components of other AGN. If this is the case then the jet in Mrk 3 is two-sided and we see no emission on either side of the nucleus for the first ~ 30 pc.

If SSA is indeed responsible for the flat radio spectrum of this component then its brightness temperature must be in excess of 10^9 K, although at present we can only place a lower limit of 3.5×10^6 K on T_B (Table 3). In order for the core to be synchrotron self-absorbed it must have

a maximum size of ~ 2 mas (~ 0.5 pc). This prediction will be tested by forthcoming VLBA observations.

3.2.2. Interpretation of the radio structures in Mrk 3

The radio source in Mrk 3 is one of the nearest known examples of an AGN containing a pair of highly-collimated radio jets. The details revealed in our new map of Mrk 3 therefore show the structure of such systems on a very small spatial scale. Here we discuss the nature of the jets in Mrk 3 based on this small-scale evidence.

General structure: As noted previously, the radio emission follows an overall ‘S’-shaped distribution. This could be due either to a change in the ejection axis of the jets with time, or else to the interaction of the jets with a rotating interstellar medium. As Figure 4 shows, the brightest optical line emission tends to be associated with the leading (convex) edge of the ‘S’ (Capetti et al. 1995a) - an observation which could favor either scenario.

The flat-spectrum core: In radio-loud sources the innermost radio components observed with VLBI are usually assumed to mark the first recollimation shocks within the jet. The identification of an unresolved flat-spectrum component in Mrk 3 therefore provides us with the best estimate of the position of the central engine. The deconvolved size of this source is < 10 pc, suggesting that the first shocks in the jet must occur within 5 pc of the central engine. Clearly an immediate goal for future VLBI would be to study this region in more detail and hopefully to resolve the core component into two recollimation shocks. Flux density comparisons might then give some clues as to the presence of relativistic velocities in the inner jet regions and the orientation of the two jets with respect to our line of sight.

The western hotspot: The hotspot itself appears to be edge-brightened, but with a complex of bright knots in the center. The overall appearance is suggestive of a shell or bowshock where the jet is interacting violently with the external medium. The knots could be the result of radio emission over a relatively large 3D interaction surface at the head of the jet which is seen in projection. Alternatively they could mark a series of increasingly violent collisions as the jet is diverted within the hotspot before finally impacting on the external medium.

A comparison of the western and eastern jets: Apart from their participation in the overall ‘S’-shaped morphology of the source, the two radio jets display a number of obvious differences. The most striking of these is the absence at the end of the eastern jet of strong radio emission and of any structure analogous to the bright western hotspot. Another obvious difference is that, unlike its western counterpart, the eastern jet contains two bright radio components within 100 pc of the nucleus.

It is tempting to suggest that these two circumstances are related. If, as suggested above, the radio knots mark the sites of shocks where oscillations in the jet direction have caused it to

strike the walls of the channel, then the presence of two strong collisions early on in the course of the eastern jet might cause much of the bulk kinetic energy of the jet material to be thermalised, leading to a large drop in the jet’s Mach number.

Radio maps at lower resolution (eg Unger et al. 1986; Kukula et al. 1993) show that beyond the structure visible in the current maps the eastern jet emission curves to the south and continues to fade. Interestingly, the HST study by Capetti et al. (1995a) shows that the line emission in this region *does not* fade but remains bright (Figure 4). However, the ionisation state here, as traced by the $[\text{OIII}]/\text{H}\alpha$ ratio, is two to three times higher than in the rest of the NLR, indicating lower gas densities. By contrast, the diffuse line emission associated with the western hotspot is relatively faint and has a low ionisation, which Capetti et al. interpret as evidence for a high-density shell of shocked material surrounding the radio lobe.

The differences in the properties of the two jets recall those between the two main types of structure found in classical radio galaxies: FR II sources, in which supersonic jets end in sharp-edged hotspots confined by shocks; and FR I, where the jets appear to become subsonic before they terminate (see, for instance, Leahy 1991). Thus the western jet in Mrk 3 is analogous to an FR II jet, maintaining a high Mach number along its length and terminating in a violent shock where it impinges on the external medium. In contrast, the eastern jet, once it has passed through the two bright knots, behaves more like an FR I source, dissipating into its surroundings without producing strong shocks. Thus, the radio source in Mrk 3, although roughly an order of magnitude less luminous than classical radio sources and confined to the nuclear regions of its host, might offer insights into both types of structure displayed by large, powerful radio galaxies. Further high-resolution work on this object, such as our own forthcoming VLBA observations, will be necessary in order to determine the spectral indices of the compact radio features more accurately, and to search for proper motions and other changes within the jet.

3.3. Markarian 231

Mrk 231 is an ultra-luminous infrared galaxy (Sanders et al. 1988), whose Seyfert 1 spectrum also contains multiple blueshifted absorption-line systems (Boksenberg et al. 1977). Boksenberg et al. also estimate 2 magnitudes of extinction towards the optical nucleus of Mrk 231, implying that the object is technically a radio-quiet quasar rather than a Seyfert galaxy, according to the luminosity criterion of Schmidt & Green (1981).

Mrk 231 possesses complex radio structure on a variety of physical scales, consisting of both compact, high-surface-brightness features and regions of more diffuse emission. At the lowest angular resolutions radio images of Mrk 231 show a bright, nuclear source with a large region of faint emission extending ~ 30 arcsec (~ 2.4 kpc) to the south (Hutchings & Neff 1987; Carilli, Wrobel & Ulvestad 1998). The nuclear radio source remains point-like at VLA resolutions (eg Kukula et al. 1995) but with VLBI the component is resolved into a small, high-surface-brightness

central component embedded in a diffuse, roughly elliptical region of emission ~ 200 mas (~ 160 pc) across (Carilli et al. 1998). Carilli et al. interpret this diffuse structure as synchrotron emission from the inner part of the molecular gas disc detected in CO by Bryant & Scoville (1996).

The compact radio source at the center of the ‘disc’ has a convex radio spectrum, and a high brightness temperature (McCutcheon & Gregory 1978; Ulvestad, Wilson & Sramek 1981; Neff & Ulvestad 1988). Neff & Ulvestad (1988), using three-station VLBI with the EVN in the early 1980s, were able to demonstrate that this component is elongated in a north-south direction, perpendicular to the major axis of the molecular disc. More recent VLBA observations have further resolved the source into a core-lobe structure (Ulvestad, Wrobel & Carilli 1998; Carilli et al. 1998) with a bright central component and southern lobe separated by ~ 30 mas (~ 20 pc), and a weaker lobe 20 mas to the north. At high frequencies the ‘core’ itself is resolved into a 2-milliarcsec (1.5-pc) triple source which is misaligned with the ‘lobes’ to the north and south (Ulvestad, Wrobel & Carilli 1998), reminiscent of the parsec-scale radio structures of NGC 1068 (Gallimore et al. 1997) and NGC 4151 (Ulvestad et al. 1998).

The lack of short baselines in the EVN means that it is most sensitive to radio structures which are intermediate in size between the small-scale (~ 30 mas) core-lobe source and the larger ~ 200 mas) ‘disc’ detected with the VLBA by Carilli et al. (1998). In the current EVN map of Mrk 231 (Figure 5) the diffuse ‘disc’ emission is resolved out, leaving only the linear nuclear source. The core-lobe structure from the VLBA maps is only partially resolved by the EVN and forms the brightest part of a somewhat larger (~ 100 pc) jet-like structure aligned in $PA \sim 20^\circ$. In addition to the VLBA source, this ‘jet’ contains two more radio components ~ 70 mas (50 pc) and 130 mas (90 pc) to the southwest.

The total flux density of the VLBA core-lobe source does not appear to have varied significantly during the six years separating the EVN and VLBA observations (94 ± 10 mJy at 1.6 GHz with the EVN in September 1990, and 100 ± 10 mJy at 1.4 GHz with the VLBA in December 1996). Our measured fluxes are also in good agreement with those of Lonsdale, Smith & Lonsdale (1993), made in September 1991 at 1.5 GHz. At higher frequencies, where the emission from the extended steep-spectrum components is less dominant, the radio source is known to be variable (McCutcheon & Gregory 1978; Ulvestad, Wilson & Sramek 1981; Neff & Ulvestad 1988).

Clearly, our understanding of this object is far from complete. The presence of structures on a variety of scales and in different orientations - the ~ 160 -pc ‘disc’ identified by Carilli et al. (1998), the ~ 50 -pc ‘jet’ seen in the current study, and the misaligned 1.5-pc nuclear triple source detected with the VLBA by Ulvestad, Wrobel & Carilli (1998) - suggest that several processes are contributing to the radio continuum emission in Mrk 231. Ulvestad, Wrobel & Carilli (1999) provide a more detailed discussion of the various radio components in this object and the relationships between them.

3.4. Markarian 463E

This object forms the eastern component of an interacting pair of galaxies. Its Seyfert 2 spectrum contains polarized broad $H\alpha$ (Miller & Goodrich 1990, Tran 1995) and, in the near infrared, broad $Pa\beta$ (Veilleux, Goodrich & Hill 1997), indicating the presence of a hidden Seyfert 1 nucleus. Mazzarella et al. (1991) infer large amounts of visual extinction towards the nucleus and speculate that, but for this, Mrk 463E would be classified as a quasar. Ground-based studies of the [OIII] emission show that the nuclear region is elongated in $PA \sim 180^\circ$ and that fainter emission fills a roughly biconical volume extending ~ 20 arcsec (~ 18 kpc) to the north and south of the nucleus (Hutchings & Neff 1989).

The object possesses radio structure on several different scales, all - like the [OIII] emission - aligned in a roughly north-south direction. Mazzarella et al. (1991) report radio components 4 arcsec (3.6 kpc) north and 18 arcsec (16.2 kpc) south of the nucleus. Strong radio emission is also associated with the nucleus itself: existing radio images (Unger et al. 1986, Neff & Ulvestad 1988, Mazzarella et al. 1991) show a bright, slightly extended radio source coincident with the optical brightness peak of the galaxy, with a second radio component lying 1.2 arcsec (1 kpc) to the south. In terms of both luminosity and overall size the radio source associated with Mrk 463E is intermediate between the sources typical of the majority of Seyfert galaxies and those found in radio galaxies and quasars.

Optical continuum imaging with the F517N and F547N filters of the HST (Uomoto et al. 1993) resolves the nuclear region, revealing a bright component ~ 500 mas across, with an optical ‘jet’ extending southwards for 820 mas (740 pc) and stopping just short of the southern radio component. Uomoto et al. attribute this radiation to a mixture of emission lines produced *in situ* and scattered light (both continuum and emission-line) from the hidden Seyfert 1 nucleus, rather than optical synchrotron emission.

At a distance of ~ 200 Mpc, the 20-mas EVN beam corresponds to a physical size of 18 pc. In our new map (Figure 6) the brightest radio source is resolved into four discrete components, all aligned in roughly the same direction as the large-scale structure. Three of the sources form a closely spaced triplet, whilst the fourth lies some 300 mas (270 pc) further south. The radio emission to the south of the optical ‘jet’ is also resolved, and is elongated in the same direction as the overall radio and optical structures. The radio components become progressively weaker as one moves southwards.

3.4.1. A new interpretation of the nucleus of Mrk 463E

The optical brightness peak of Mrk 463E has a Type 2 (narrow line) spectrum and has traditionally been assumed to mark the site of the supermassive black hole responsible for the activity in this object. Since the brightest radio component in Mrk 463E is roughly coincident

with the optical peak it followed that this was the radio source associated with the obscured central engine. However, in other Seyferts with prominent linear radio structures this is not always the case; in both Mrk 3 (Kukula et al. 1993; this paper) and Mrk 6 (Kukula et al. 1996) the brightest radio component occurs at the end of the jet furthest from the nucleus, is resolved, edge-brightened, and has a steep radio spectrum - all the hallmarks of a ‘hotspot’ where the jet material is ploughing into the ISM of the host galaxy. In both cases, the radio emission is associated with enhanced narrow-line emission, which appears to surround the radio structure like a shell or halo. In Mrk 3 the hidden central engine is associated with an unresolved, flat-spectrum radio component. In Mrk 6, the Seyfert 1 nucleus does not appear to coincide with any of the detected radio components. Roy et al. (1994) invoked free-free absorption by ionized gas in the narrow line region to explain the lack of compact nuclear radio sources in their sample of Seyfert 1s (in Seyfert 2s we observe the object ‘side on’ and so the depth of ionized gas between the observer and the central engine is much reduced). The same mechanism might also account for the absence of a radio component at the position of the Type 1 nucleus in Mrk 6.

Tremonti et al. (1996) used HST imaging polarimetry to locate the hidden Seyfert 1 nucleus in Mrk 463E. They report that the magnetic polarization vectors converge on the southern tip of the optical ‘jet’, indicating that this, and not the bright narrow-line region north of the ‘jet’, is the true site of the central engine in this object.

The detailed radio structure of Mrk 463E revealed by our new EVN observations, when considered in conjunction with the optical structures reported by Uomoto et al. (1993), lends strong support to this finding. In Figure 7 we show the current 18-cm radio map (greyscale) superimposed on the HST continuum image by Uomoto et al. (contours). There is some question as to the positional accuracy of the two images. The radio data has undergone self-calibration, causing the absolute positional information to be lost. More seriously, HST pointing is generally only accurate to within ~ 1 arcsec, and the true pixel scale of the HST Planetary Camera image may be slightly different from the canonical value of $43.9 \text{ mas pixel}^{-1}$. In performing the registration of the two images we have forced the brightness peaks to coincide. Several aspects of the argument set out below rely heavily on this assumption, so it is clearly imperative that more accurate radio and, particularly, optical astrometry be carried out on this object.

The overall outline of the optical emission in the HST image is roughly wedge-shaped, with its apex at or near the southern radio component, 1.2 arcsec from the presumed ‘Seyfert 2 nucleus’. The enhanced optical emission forming the ‘jet’ begins immediately north of this radio component and continues north for almost a kiloparsec, incorporating three bright knots, before terminating abruptly. A gap of ~ 0.1 arcsec (90 pc) separates the ‘jet’ from the bright, resolved ‘nucleus’ to the north and a second radio component appears to lie in the gap.

Our suggested interpretation of Mrk 463E is that the ‘Seyfert 2 nucleus’ at the northern end of the jet is in fact a region of enhanced narrow-line emission associated with a radio hotspot. In accordance with the data of Tremonti et al. (1996) we suggest that the central engine itself lies

at the southern end of the optical jet, although for the reasons outlined below we feel that it is unlikely to be exactly coincident with the southern radio component. The overall wedge-shape of the extended optical emission can be accounted for by shadowing of the radiation field of the AGN by an optically-thick torus surrounding the central engine - the favored model for several other Seyferts with similar optical morphologies (*eg* Wilson & Tsvetanov 1994).

We interpret the linear optical feature seen in the HST image as an expanding cylindrical sheath or halo of material surrounding the channel of the radio jet. Such a model was suggested by Capetti and co-workers to explain the very similar structures seen in emission lines in several Seyferts, including Mrk 3 & 6 (Capetti et al. 1995a, & b, 1996). The material in the halo has been pushed aside by the passage of the radio plasma, and is subsequently ionized by UV photons from the central engine. The high density of the halo relative to the surrounding gas also makes it a more effective site for scattering of the nuclear continuum. Uomoto et al. (1993) claim that the F547M to F517N flux ratio of the ‘jet’ indicates a mixture of optical continuum and emission lines. This can be explained in our model by contributions from line emission produced *in situ* by the swept-up, ionized gas, as well as polarized continuum and broad permitted line emission (already detected by Miller & Goodrich 1990) from the obscured nucleus which have been scattered into our line of sight by electrons in the halo. Double-peaked line profiles would be indicative of an expanding cylindrical sheath of material. Free-free continuum emission from shocked gas in the halo might also be present. Optical spectroscopy and spectropolarimetry with high spatial resolution will be required in order to determine the precise contributions from each mechanism.

The estimated lifetime for λ 18cm synchrotron-emitting electrons in this source (derived from the minimum energy magnetic field values listed in Table 2) is $\sim 10^4$ years. Hence, unless the bulk velocity of the jet is an appreciable fraction of the speed of light ($\geq 0.01c$) the electrons in the plasma will radiate most of their energy before traveling more than a few tens of parsecs from the origin of the jet. At larger distances a fresh injection of energy will be required in order to produce appreciable amounts of synchrotron emission. We would therefore expect to detect strong synchrotron emission at sites where the jet plasma is interacting violently with its surroundings, leading to the re-acceleration of electrons, but very little where the jet is flowing freely.

Thus, in the region of the optical ‘jet’ the plasma has already drilled out a channel for itself, through which it flows relatively unimpeded, and produces little or no synchrotron emission. The radio emission immediately north of the linear optical feature might indicate that the jet is colliding with an obstacle at this point. It is not clear why the optical emission should simultaneously fall in brightness, but Taylor, Dyson & Axon (1992) point out that the shocks produced by the collision of a jet with an external medium can heat the swept-up material to temperatures $\gg 10^4\text{K}$, too large for the emission of forbidden lines to occur.

Following this encounter, which appears to alter the course of the jet, the plasma feeds into the bright radio hotspot. This is the site at which the jet is actively carving a channel into the local ISM. The observed radio structure of the hotspot consists of three successively brighter

components, the first two of which are compact and a third which is resolved in a direction roughly orthogonal to that of the jet. We suggest that these features are analogous to the internal radio structure observed in the western hotspot of Mrk 3 (Figure 2) and that the bright transverse feature is associated with a bowshock at the head of the jet. Mazzarella et al. (1991) detected ~ 320 mJy of emission in this region with the VLA at 20 cm, implying that over 100 mJy of extended flux has been ‘resolved out’ by the small beam of the EVN. The VLA map by Mazzarella et al. also contains a weak radio component 4 arcsec (3.6 kpc) north of the nucleus. This could indicate either that the jet is not entirely disrupted in the structure which we have dubbed the hotspot, or else that the hotspot was formed when dense material drifted into the path of the jet, cutting off the radio structure further to the north.

Unger et al. (1986) found that the radio emission in Mrk 463E has a steep spectrum between 408 and 1666 MHz. Although the angular resolution of their maps was not sufficient to resolve the individual knots which make up the northern component, a steep radio spectrum in this region lends credence to our suggestion that this is a radio hotspot rather than the central engine itself. The radio component to the south of the optical ‘jet’ also has a steep spectrum and the emitting region is resolved in our EVN map. This makes it unlikely to be directly associated with the central engine, since the nuclear components observed in other Seyferts tend to be compact, with flat spectra.

However, further evidence that the true nucleus is located in this vicinity is the mention by Neff & Ulvestad (1988) of a region of extremely blue optical continuum emission apparently coincident with the southern radio component (in our EVN map). We suggest that this blue emission might be a signature of the hidden Seyfert 1 nucleus. New studies of the broad-line emission from Mrk 463E (polarized $H\alpha$ in the optical and broad $Pa\beta$ in the near infrared) with improved spatial resolution would also assist in defining the scattering geometry and locating the central engine.

Mazzarella et al. (1991) also found a knot of radio emission 18 arcsec (16.2 kpc) south of the nucleus in their 20 cm VLA image, which could be construed as a radio hotspot at the end of a southern counterpart of the jet in the north (although, of course, it might equally well be entirely unrelated to the AGN). The relative weakness of the radio emission in this component, and the lack of any detectable emission from the counterjet itself, might be explained in a number of ways.

If the counterjet is directed away from us, into the plane of the sky, and the bulk velocity is relativistic then Doppler dimming could lead to a reduction in the observed radio emission. A difference in the environment to the south of the nucleus might also lead to less radio emission: if the counterjet encounters little resistance from the ISM then there will be few opportunities for the re-acceleration of electrons and a corresponding absence of synchrotron radiation. A lower density in the southern ISM would also account for the greater length of the counterjet (16 kpc) relative to the maximum extent of the northern radio emission (3.6 kpc). Certainly, in view of the disturbed nature of the Mrk 463 system, we would not necessarily expect the galaxy’s density

contours to be symmetrical about the nucleus of Mrk 463E.

A final possibility is that the counterjet is currently dormant or inactive and the southern radio component is therefore the fading remnant of a more luminous hotspot.

The ground-based [OIII] image by Hutchings & Neff (1989) shows a fan-shaped region of emission extending ~ 20 arcsec to the north of the nucleus. However, to the south the [OIII] emission is concentrated in a bright, resolved knot at a distance of ~ 10 arcsec from the nucleus, with little extended emission. This could indicate either larger amounts of obscuration between the Earth and the ionized gas to the south (perhaps because the southern cone of ionising photons is directed away from us) or else, once again, a lack of gas in this region.

However, at this stage we cannot rule out the possibility that much of the faint [OIII] and radio emission on arcsecond scales is associated with starforming regions rather than the central engine of Mrk 463E.

To summarize: we suggest that the optical and radio brightness peak in Mrk 463E has been mistakenly identified as the location of the active nucleus in this object, when in fact it represents the working surface of a jet, which originates ~ 1 arcsec to the south. Since our understanding of this object depends crucially on the ability to match up high-resolution images made in many different regions of the spectrum, more accurate astrometry at all wavelengths is urgently required.

4. Discussion

Three of the objects in our study (Mrk 3, 231 and 463E) were observed previously with the EVN in the early 1980s at 1.6 GHz (Neff & Hutchings 1988). Our maps agree with the previous data in terms of the overall morphology of the sources but advances in instrumentation and software have resulted in significant improvements in image quality and the new maps therefore contain much more detail.

Most of the compact radio emission in all four Seyferts has a steep radio spectrum (component 4 in Mrk 3 has a flat spectrum) and is clearly non-thermal in origin. Neff & Ulvestad (1988) point out that unrealistically large supernova rates would be required in order to reproduce the radio luminosities observed in the compact radio components of Mrk 3, 231 and 463; based on our current measurements the same appears to be the case for Mrk 1. Moreover, the combination of high ($\geq 10^5$ K) brightness temperatures and steep radio spectra appears to rule out supernovae as the primary source of the synchrotron emission since, in a starburst complex, brightness temperatures would be limited to $\leq 10^5$ K and one would expect the radio spectrum to flatten for $T_B > 10^4$ K (see Condon 1992).

An AGN is therefore the most likely source of the VLBI radio emission, and in three of the objects we have mapped, the radio morphology also strongly suggests the presence of less powerful forms of the jets found in radio-loud sources. However, there is evidence for galaxy

interactions/mergers in all four cases, and the more diffuse and amorphous radio emission (for example, that detected on arcsecond scales in Mrk 231 by Hutchings & Neff 1987, or the radio halo in Mrk 1) may well be the result of starburst activity rather than a direct product of the AGN.

What can be learned from these four objects? We cannot hope to draw generalized conclusions about Seyferts as a class from such a small sample. Also, optical imaging and kinematical studies indicate that all four objects in our study are currently interacting with neighboring galaxies (Mrk 1, 3 & 463E) and/or have recently undergone mergers (Mrk 3 & 231). Though such processes may well play a rôle in triggering and fueling the activity in all active galaxies (*eg* Phinney 1994), the prominent disturbances in these four galaxies might account for some of the complexity in their radio structures. However, the current observations do highlight a number of important points which should be taken into account in any consideration of Seyfert radio properties.

With very high angular resolution, jet-like structures *can* be found even in compact Type 1 objects such as Mrk 231, in which the axis of the central engine is probably aligned quite closely with the line of sight. The presence of large-scale (> 100 pc) collimated radio jets in Mrk 3 and 463E also serves to reinforce the message that Seyfert 1s are capable of producing such structures since, although these two objects have Type 2 spectra as observed from our own vantage point, spectropolarimetry and infrared spectroscopy indicate that both contain a hidden Type 1 nucleus.

On the other hand, there are Seyferts such as Mrk 1 which, although they possess respectably luminous radio sources, show no signs of jet-like structure on scales as small as a few parsecs. Mrk 1 is a particularly good example of this class because, as a Type 2 Seyfert, the unified model predicts that the ejection axis for a putative radio jet should be close to the plane of the sky, thus minimizing any projection effects. It is interesting to note that, in the present sample, both of the Type 2 Seyferts which show evidence for a hidden Type 1 nucleus also contain radio jets, whilst Mrk 1, in which all attempts to find broad lines have so far failed, does not.

It appears that whilst some Seyfert galaxies of both types are certainly capable of producing linear, jet-like radio sources, the radio structures in Seyferts can range in size from extremely small (< 10 pc) nuclear sources through to jets on scales of tens, hundreds and even thousands of parsecs. This large distribution of sizes is intrinsic to the Seyfert population and is quite separate from viewing angle effects. Possibly the radio jets in Seyferts are relatively short-lived compared to the lifetime of the active nucleus, so that when we observe a sample of objects, we see jets in various stages of development, as well as objects in which jets are not currently active. Alternatively, there may be some Seyferts of both spectral types which are simply incapable of producing radio jets, perhaps due to environmental factors such as the gas density/kinematics in the nuclear region of the host galaxy and the orientation of the central engine relative to the plane of the host.

The factors at work in the host galaxy (dust and gas content, interaction and star-formation history) and the active nucleus (immediate environment and orientation of the central engine, the size, age and morphology of the radio source), as well as the biases and omissions introduced by

observational constraints, combine to make the observed properties of a particular Seyfert galaxy distinctive and unique. This point is illustrated by the cases of Mrk 3 and 463E, in which jet and counterjet have very different appearances due, perhaps, to the different conditions which they encounter *en route*. One should not forget that Seyfert galaxies are complicated systems composed of many elements, whose properties can change and evolve on relatively short timescales. Consequently one should not be too surprised if simplistic models fail on some level when applied globally to large samples of objects.

Further studies of the relationship between the AGN and its host need to be carried out before we can be confident about our interpretation of Seyfert radio surveys. High-resolution imaging at many wavelengths will clearly play a major rôle in such studies, but, as the present work demonstrates, accurate astrometry will be crucial in order to match up the different datasets.

5. Summary

The maps presented here clearly demonstrate that VLBI can be a highly effective tool for investigating the radio structures of Seyfert nuclei, even though the radio emission from these objects is relatively weak when compared to radio-loud sources. Since Seyferts are in general much closer to us than other types of AGN, the spatial resolution achieved by VLBI is unprecedented, allowing us to study the structure of the radio jets on scales of a few parsecs and to investigate in detail the complex interactions between the jets and their environment.

Radio jets exist in both broad- and narrow-line Seyferts, although the scale of such structures varies from a few tens of parsecs to several kiloparsecs. The range in sizes appears to be intrinsic to the Seyfert population and is independent of any additional projection effects caused by the orientation of the central engine. However, there are also objects which possess luminous nuclear radio sources yet which show no evidence for jets, even on scales of ≤ 10 pc.

In Mrk 3 and 463E we find evidence for jets containing internal shocks and terminating in luminous, edge-brightened hotspots resembling the structures seen in large-scale FR II radio sources. However, in general the observed radio properties of an individual Seyfert nucleus are likely to be a complex function of the local environment as well as of the central engine itself, making each object unique. This has important consequences for the interpretation of radio surveys of Seyferts.

The authors would like to thank Bill Junor for help in reducing the data, Ant Holloway for producing Figure 4, Christina Tremonti and Alan Uomoto for useful discussions on the subject of Mrk 463, and Ger de Bruyn, George Miley and Dave Graham for their invaluable contribution to the early stages of this project. We are also grateful to James Ulvestad, the referee, whose comments resulted in significant improvements to this paper. MJK acknowledges PPARC support and STScI funding (grant number O0573). The EVN is a large-scale facility of the European

Union and is administered by the European Consortium for VLBI. MERLIN is a national facility operated by the University of Manchester on behalf of PPARC. This research has made use of the NASA/IPAC Extragalactic Database (NED) which is operated by the Jet Propulsion Laboratory, California Institute of Technology, under contract with the National Aeronautics and Space Administration.

REFERENCES

- Boksenberg, A., Carswell, R. F., Allen, D. A., Fosbury, R. A. E., Penston, M. V. & Sergent, W. L. W. 1977, MNRAS, 178, 451
- Braatz, J. A., Wilson, A. S., & Henkel, C. 1994, ApJ, 437, L99
- Bryant, P. M., & Scoville, N. Z., 1996, ApJ, 457, 678
- Capetti, A., Macchetto, F., Axon, D. J., Sparks, W. B., & Boksenberg, A. 1995a, ApJ, 448, 600
- Capetti, A., Axon, D. J., Kukula, M., Macchetto, F., Pedlar, A., Sparks, W. B., & Boksenberg, A. 1995b, ApJ, 454, L85
- Capetti, A., Axon, D. J., Macchetto, F., Sparks, W. B., & Boksenberg, A. 1996, ApJ, 469, 554
- Clements, E. D. 1981, MNRAS, 197, 829
- Carilli, C. L., Wrobel, J. M., & Ulvestad, J. S., 1998, ApJ, 115, 928
- Condon, J. J. 1992, in AIP Conference Series 254, Testing the AGN Paradigm, ed. S. S. Holt, S. G. Neff & C. M. Urry (New York: AIP), 629
- Gallimore, J. F., Baum, S. A., & O’Dea, C. P., 1997, Nature, 388, 852
- Ghosh, T., Schilizzi, R. T., Miley, G. K., de Bruyn, A. G., Kukula, M. J., Pedlar, A., Graham, D., & Saikia, D. G. 1994, in IAU Symposium 159, Multi-wavelength continuum emission of AGN, ed. T. J. -L. Courvoisier & A. Blecha (Dordrecht: Kluwer), 426
- Halkides, D., Ulvestad, J., & Roy, A., 1997, BAAS, 29, 1375
- Huchra, J. P., & Burg, R. 1992, ApJ, 393, 90
- Hutchings, J. B., & Neff, S. G. 1987, AJ, 93, 14
- Hutchings, J. B., & Neff, S. G. 1989, AJ, 97, 1306
- Kay, L. E. 1994, ApJ, 430, 196
- Keel, W. C. 1996, AJ, 111, 696

- Kukula, M. J., Ghosh, T., Pedlar, A., Schilizzi, R. T., Miley, G. K., de Bruyn, A. G. & Saikia, D. J. 1993, MNRAS, 264, 893
- Kukula, M. J., Pedlar, A., Baum, S. A., & O’Dea, C. P. 1995, MNRAS, 275, 67
- Kukula, M. J., Holloway, A. J., Pedlar, A., Meaburn, J., Lopez, J. A., Axon, D. J., Schilizzi, R. T., & Baum, S. A. 1996, MNRAS, 280, 1283
- Leahy, J. P., 1991, in Beams and Jets in Astrophysics, ed. P. A. Hughes, (Cambridge: CUP), p175
- Lonsdale, C. J., Smith, H. E., & Lonsdale, C. J., 1993, ApJ, 405, L9
- Mazzarella, J. M., Gaume, R. A., Soifer, B. T., Graham, J. R., Neugebauer, G., & Matthews, K. 1991, AJ, 102, 1241
- McCutcheon, W. H., & Gregory, P. C. 1978, AJ, 83, 566
- Miley, G. 1980, ARA&A, 18, 165
- Miller, J. S., & Goodrich, R. W. 1990, ApJ, 355, 456
- Mulchaey, J. S., & Wilson, A. S. 1995, ApJ, 455, L17
- Mundell, C. G., Wrobel, J., Pedlar, A., & Gallimore, J., 1997, BAAS, 29, 1252
- Neff, S. G., & Ulvestad, J. S. 1988, AJ, 96, 841
- Oosterloo, T. , Tzioumis, A., Reynolds, J., Morganti, R., Tsvetanov, Z., McCulloch, P., & King, E., 1998, in IAU Colloquium 164: Radio Emission from Galactic and Extragalactic Compact Sources, ASP Conference Series Vol. 144, ed. J. A. Zensus, G. B. Taylor, & J. M. Wrobel, (San Francisco: ASP), p197
- Pedlar, A., Kukula, M. J., Longley, D. P. T., Muxlow, T. B., Axon, D. J., Baum, S., O’Dea, C., & Unger, S. W. 1993, MNRAS, 263, 471
- Phinney, E. S. 1994, in Mass Transfer Induced Activity in Galaxies, ed. I. Shlosman (Cambridge: CUP), 1
- Roy, A. L., Norris, R. P., Kesteven, M. J., Troup, E. R., & Reynolds, J. E. 1994, ApJ, 432, 496
- Roy, A. L., Ulvestad, J. S., Colbert, E. J. M., Wilson, A. S., & Norris, R. P., 1998, in IAU Colloquium 164: Radio Emission from Galactic and Extragalactic Compact Sources, ASP Conference Series Vol. 144, ed. J. A. Zensus, G. B. Taylor, & J. M. Wrobel, (San Francisco: ASP), p301
- Rush, B., Malkan, M. A., & Spinoglio, L. 1993, ApJS, 89, 1

- Sanders, D. B., Soifer, B. T., Elias, J. H., Madore, B. F., Matthews, K., Neugebauer, G., & Schoville, N. Z. 1988, *ApJ*, 325, 74
- Schmidt, M., & Green, R. F. 1981, *ApJ*, 269, 352
- Schmidt, G. D., & Miller, J. S. 1985, *ApJ*, 290, 517
- Taylor, D., Dyson, J. E., & Axon, D. J. 1992, *MNRAS*, 255, 351
- Thean, A., Pedlar, A., Kukula, M. J., & Baum, S. A. 1998, in preparation
- Tran, H. D. 1995, *ApJ*, 440, 565
- Tremonti, C. A., Uomoto, A., Antonucci, R. R. J., Tsvetanov, Z. I., Ford, H. C., & Kriss, G. A., 1996, *BAAS*, 28, 1287
- Ulvestad, J. S., Wilson, A. S., & Sramek, R. A. 1981, *ApJ*, 247, 419
- Ulvestad, J. S., & Wilson, A. S. 1984a, *ApJ*, 278, 544
- Ulvestad, J. S., & Wilson, A. S. 1984b, *ApJ*, 285, 439
- Ulvestad, J. S., Wrobel, J. M., & Carilli, C. L., 1998, in *IAU Colloquium 164: Radio Emission from Galactic and Extragalactic Compact Sources*, ASP Conference Series Vol. 144, ed. J. A. Zensus, G. B. Taylor, & J. M. Wrobel, (San Francisco: ASP), p199
- Ulvestad, J. S., Wrobel, J. M., & Carilli, C. L., 1999, *ApJ*, in press
- Ulvestad, J. S., Roy, A. L., Colbert, E. J. M., & Wilson, A. S., 1998, *ApJ*, 496, 196
- Unger, S. W., Pedlar, A., Boller, R. V., & Harrison, B. A. 1986, *MNRAS*, 219, 387
- Uomoto, A., Caganoff, S., Ford, H. C., Rosenblatt, E. I., Antonucci, R. R. J., Evans, I. N., & Cohen, R. D. 1993, *AJ*, 105, 1308
- Veilleux, S., Goodrich, R. W., & Hill, G. J. 1997, *ApJ*, 477, 631
- Wilson, A. S., & Tsvetanov, Z. I. 1994, *AJ*, 107, 1277

Fig. 1.— 18-cm EVN map of Mrk 1. The beam is $0.024'' \times 0.018''$ in PA 71° (indicated by the ellipse in the lower left hand corner of the map), equivalent to a spatial resolution of ~ 6 pc. (Peak flux density = 31 mJy beam^{-1} ; n^{th} contour is $0.14 \times 2^{n-1} \text{ mJy beam}^{-1}$.)

Fig. 2.— Top: 18-cm EVN+MERLIN map of Mrk 3. The beam is $0.027'' \times 0.023''$ in PA 51° , equivalent to a spatial resolution of ~ 5 pc. Peak flux density = $34.4 \text{ mJy beam}^{-1}$; 3σ noise is $0.2 \text{ mJy beam}^{-1}$, with contours at -1, 1, 5, 10, 15, 20, 25, 30, 40, 50, 75, 100, 150 & 300 times this value. The cross marks the position of the optical nucleus as determined by Clements (1981). Bottom: Cartoon of the radio emission in Mrk 3, showing the distribution of the extended emission (solid lines) and the most prominent compact radio features (shaded regions). The numbering scheme is modified from that used to describe the original 6-cm MERLIN map (Kukula et al. 1993).

Fig. 3.— Spectral index map of Mrk 3. The spectral index, α (defined by $S \propto \nu^\alpha$), is indicated by the greyscale bar at the top of the frame. The measurements were made between 1.6 and 4.8 GHz by comparing the current EVN+MERLIN data with the 4.8-GHz MERLIN map by Kukula et al. (1993). The two maps were convolved with an identical $0.09'' \times 0.07''$ beam. The cross marks the peak of the optical emission, as determined by Clements (1981).

Fig. 4.— [OIII] emission in the nucleus of Mrk 3 (greyscale) imaged with the HST by Capetti et al. (1995a) through the F501N filter, with the 18-cm radio emission (contours) superimposed. Note the bright knot of [OIII] to the south of the eastern radio jet, and also how the line emission appears to favour the convex edge of the S-shaped curvature. As before, the cross marks the peak of the optical continuum emission, as determined by Clements (1981), which appears to be offset from the hidden Seyfert 1 nucleus by ~ 200 mas.

Fig. 5.— 18-cm EVN map of Mrk 231. At a distance of 164 Mpc the $0.029'' \times 0.021''$ (PA 54°) beam is equivalent to a spatial resolution of ~ 15 pc. (Peak flux density = 75 mJy beam^{-1} ; n^{th} contour is $0.7 \times 2^{n-1} \text{ mJy beam}^{-1}$.)

Fig. 6.— 18-cm EVN map of Mrk 463E. The beam has a FWHM of $0.023'' \times 0.022''$ in PA 49° , equivalent to a spatial resolution of ~ 18 pc. (Peak flux density = 38 mJy beam^{-1} ; n^{th} contour is $0.6 \times 2^{n-1} \text{ mJy beam}^{-1}$.)

Fig. 7.— 18-cm EVN map of Mrk 463E (greyscale; scale bar marked in mJy beam^{-1}) with the HST optical continuum (F517M filter) image by Uomoto et al. (1993) superimposed (contours). The registration of the two datasets was performed by forcing the optical and radio brightness peaks to coincide. The radio map has been convolved with a gaussian function to give it a comparable resolution to the HST image (~ 50 mas).

Table 1. Objects in the current sample. Optical positions are taken from Clements (1981) and refer to the peak of the optical continuum emission. Dates for the 18-cm EVN observations reported in this paper are listed as day/month/year (additional 18-cm observations of Mrk 3 were made with MERLIN on 26/04/93).

Object	Seyfert Type	cz (km s ⁻¹)	Optical position of nucleus (B1950)		Observing date	Alternative name
			RA ($h\ m\ s$)	Dec ($^{\circ}\ ' \ ''$)		
Mrk 1	2	4800	01 13 19.616 \pm 0.009	+32 49 33.12 \pm 0.11	27/09/90	NGC 449
Mrk 3	2	4110	06 09 48.419 \pm 0.023	+71 03 10.72 \pm 0.11	01/10/90	UGC 3426
Mrk 231	1	12300	12 54 05.004 \pm 0.012	+57 08 38.26 \pm 0.10	30/09/90	UGC 8058
Mrk 463	2	15150	13 53 39.858 \pm 0.007	+18 36 57.92 \pm 0.10	30/09/90	UGC 8850

Table 2. Radio properties of Mrk 1, 231 and 463. The error in the measured flux densities due to calibration uncertainty is estimated to be $\sim 10\%$. Values for the magnetic field, energy density and pressure in the radio plasma were estimated using minimum energy arguments (Miley 1980), and are given in the following units: B_{eq} 10^{-7} T; U_{eq} 10^{-8} J m $^{-3}$; P_{eq} 10^{-9} N m $^{-2}$. We have assumed spectral indices of $\alpha = -0.7$, where $S \propto \nu^\alpha$.

	Radio position (B1950)		18-cm flux density (mJy)		rms noise (mJy)	Component size (arcsec 2)	PA ($^\circ$)	Equipartition parameters			Brightness temperature (K)
	RA (<i>h m s</i>)	Dec ($^\circ$ ' ")	Peak	Total				B_{eq}	U_{eq}	P_{eq}	
Mrk 1	01 13 19.5800	+32 49 32.500	29.5	34.0	0.14	0.010×0.006	78	5.3	26.4	87.9	2.9×10^8
Mrk 231	12 54 05.0000	+57 08 38.098	74.7	94.3	0.26	0.018×0.006	20	4.2	16.5	55.1	4.5×10^8
	12 54 04.9969	+57 08 38.038	13.2	20.6	0.26	0.023×0.012	168	1.9	3.5	11.6	4.2×10^7
	12 54 04.9963	+57 08 37.970	2.2	2.6	0.26	$\sim 0.030 \times 0.020$	~ 90	0.8	0.5	1.8	2.3×10^6
Mrk 463	13 53 39.8500	+18 36 57.599	34.3	62.7	0.19	0.024×0.017	148	2.1	4.2	13.9	8.2×10^7
	13 53 39.8488	+18 36 57.546	6.3	11.6	0.19	0.021×0.020	159	1.3	1.5	5.2	1.5×10^7
	13 53 39.8486	+18 36 57.517	4.3	4.4	0.19	$< 0.017 \times 0.017$	180	> 1.2	> 1.3	> 4.3	$> 8.5 \times 10^6$
	13 53 39.8525	+18 36 57.336	3.6	13.0	0.19	$\sim 0.100 \times 0.050$	~ 180	0.5	0.2	0.7	1.4×10^6
	13 53 39.8534	+18 36 56.356	2.3	7.3	0.19	$\sim 0.100 \times 0.050$	~ 180	0.4	0.1	0.5	8.0×10^5

Table 3. Radio properties of Mrk 3 with radio components numbered as in Figure 5. The beam has a FWHM of $0.027'' \times 0.023''$ in PA 51° and the RMS noise in the map is $0.08 \text{ mJy beam}^{-1}$. Spectral indices were calculated by comparing the current data with the 6-cm map of Kukula et al. (1993) (see Figure 3). Values for the magnetic field, energy density and pressure in the radio plasma were estimated using minimum energy arguments (Miley 1980) and are given in the following units: $B_{eq} \text{ } 10^{-7} \text{ T}$; $U_{eq} \text{ } 10^{-8} \text{ J m}^{-3}$; $P_{eq} \text{ } 10^{-9} \text{ N m}^{-2}$.

	Radio position (B1950)		18-cm flux density (mJy)		Spectral index α	Component size (arcsec ²)	PA ($^\circ$)	Equipartition parameters			Brightness temperature (K)
	RA (h m s)	Dec ($^\circ$ ' ")	Peak	Total				B_{eq}	U_{eq}	P_{eq}	
1a	06 09 48.6105	+71 03 10.488	1.8	6.7	?	0.100×0.070	~ 180	0.5	0.2	0.7	5.2×10^5
1	06 09 48.5497	+71 03 10.608	2.5	45.4	-2.0	0.270×0.150	~ 90	1.4	1.8	5.9	6.1×10^5
2	06 09 48.4988	+71 03 10.576	9.7	41.8	-1.0	0.061×0.036	101	1.6	2.5	8.2	1.0×10^7
3	06 09 48.4742	+71 03 10.544	8.7	40.3	-0.5	0.067×0.036	94	1.1	1.2	4.0	9.0×10^6
4	06 09 48.4249	+71 03 10.488	5.4	9.4	-0.1	$< 0.038 \times 0.038$	180	> 1.0	> 1.0	> 3.3	$> 3.5 \times 10^6$
5a	06 09 48.3937	+71 03 10.448	2.5	3.4	-1.8	0.015×0.008	140	6.5	39.0	130.0	1.5×10^7
5b	06 09 48.3838	+71 03 10.464	4.7	7.5	-1.8	0.037×0.017	140	4.0	14.0	48.0	6.4×10^6
5c	06 09 48.3641	+71 03 10.456	2.2	4.2	-1.8	0.023×0.019	149	4.0	15.0	49.0	5.2×10^6
5d	06 09 48.3510	+71 03 10.448	2.3	3.3	-1.8	0.040×0.020	~ 180	2.8	7.4	24.7	2.2×10^6
6a	06 09 48.3214	+71 03 10.400	2.1	10.7	-0.9	0.070×0.040	~ 135	0.9	0.7	2.3	2.1×10^6
6b	06 09 48.3116	+71 03 10.400	4.1	7.5	-0.9	0.037×0.034	140	1.1	1.2	3.9	3.2×10^6
6c	06 09 48.3050	+71 03 10.376	3.2	3.9	-0.9	0.010×0.007	151	3.2	9.4	31.0	3.0×10^7
7	06 09 48.2738	+71 03 10.424	2.6	6.3	-0.4	0.039×0.027	17	9.6	0.9	2.8	3.2×10^6
8a	06 09 48.1966	+71 03 10.464	11.6	41.7	-1.2	0.070×0.050	~ 135	1.7	2.5	8.5	6.4×10^6
8b	06 09 48.1834	+71 03 10.416	19.7	27.9	-1.2	0.058×0.048	19	1.6	2.5	8.3	5.4×10^6
8c	06 09 48.1801	+71 03 10.408	22.9	32.4	-1.23	0.062×0.043	66	1.7	2.8	9.3	6.6×10^6
8d	06 09 48.1686	+71 03 10.432	34.4	124.3	-1.2	0.091×0.044	25	2.1	4.1	14.0	1.7×10^7

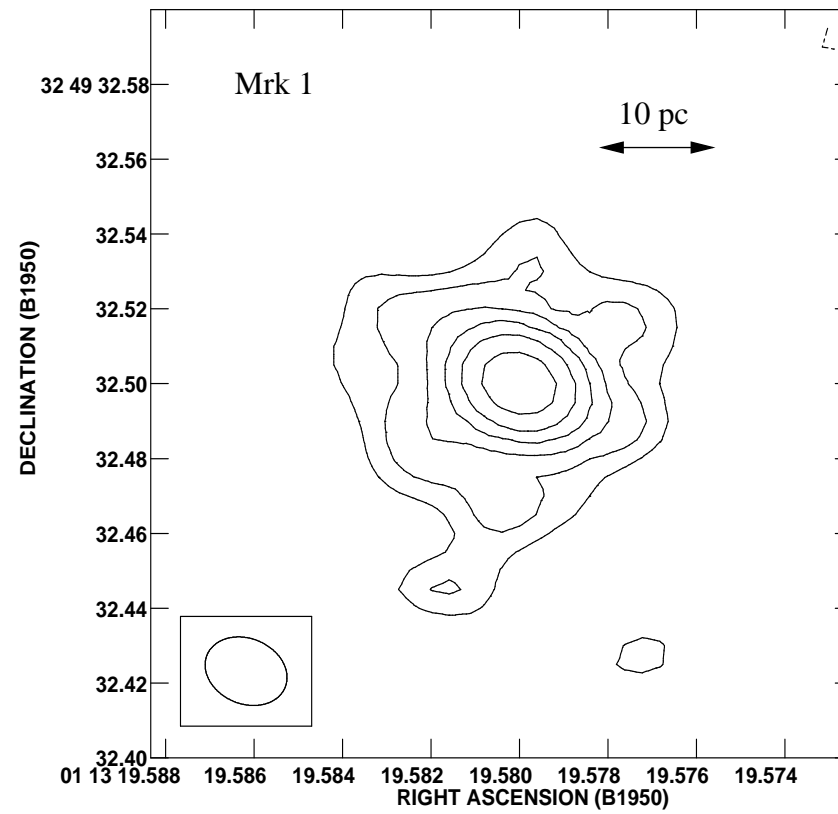


Figure 1

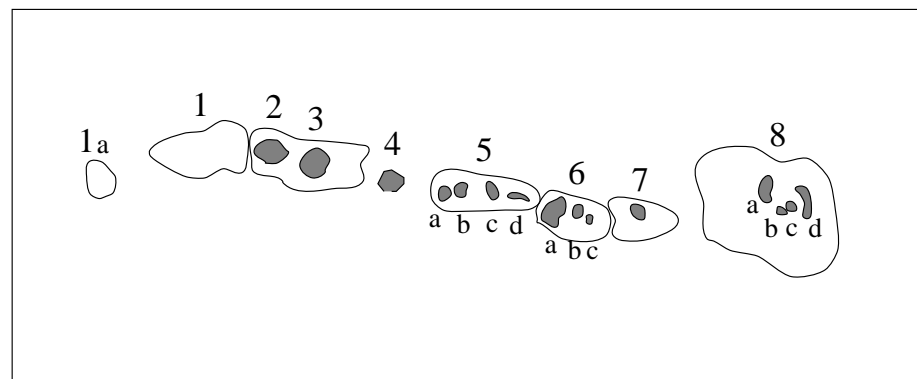
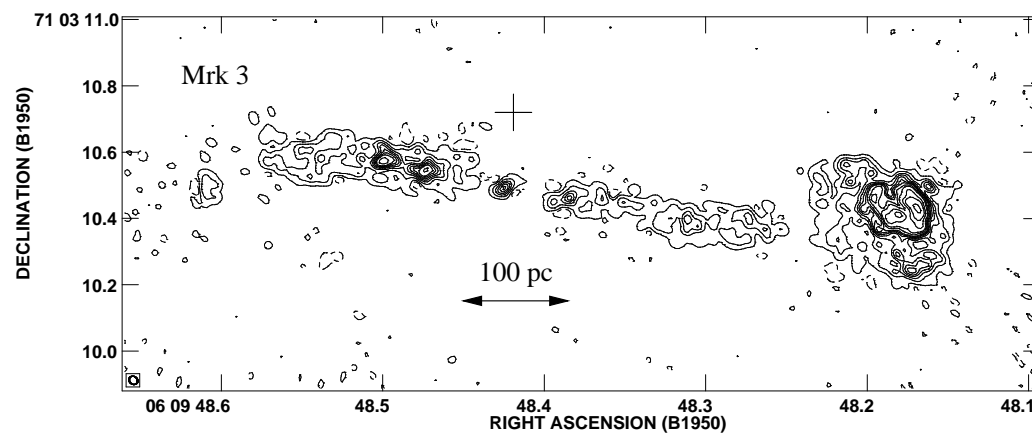


Figure 2

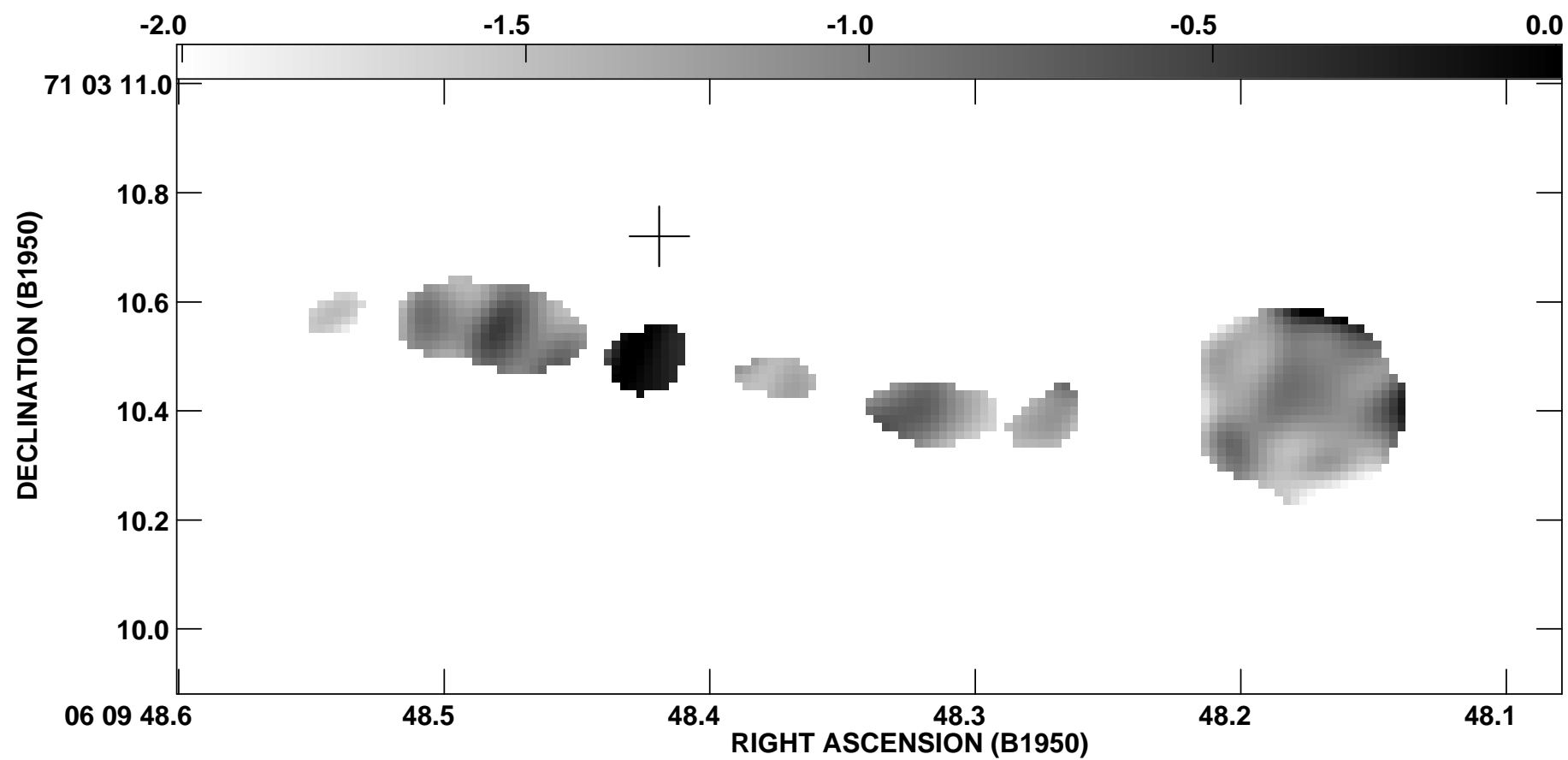


Figure 3

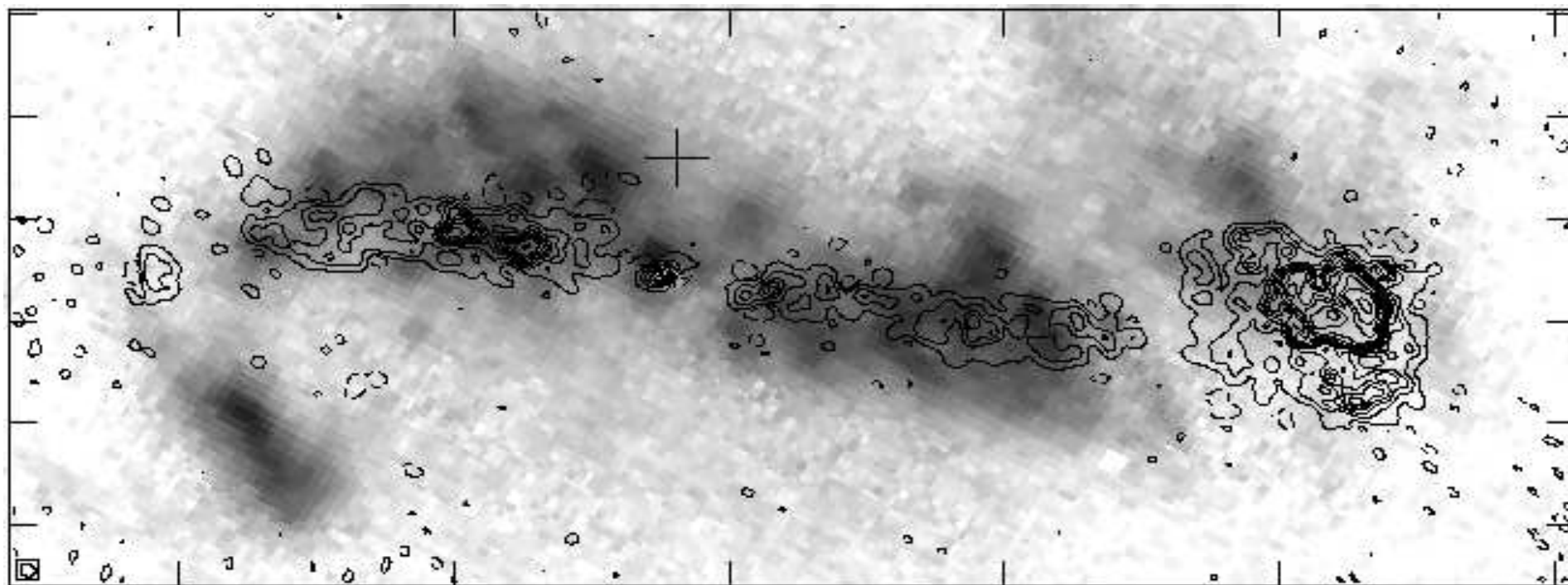


Figure 4

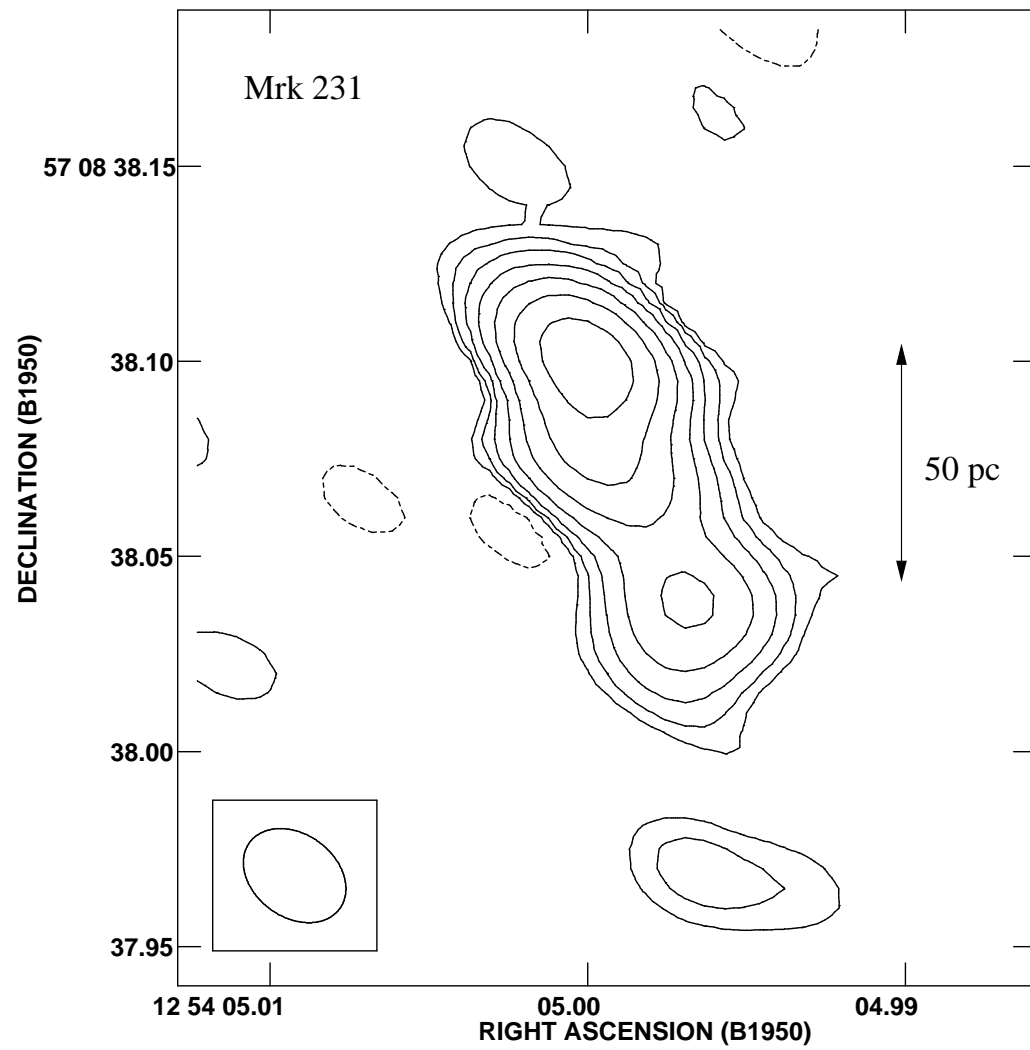


Figure 5

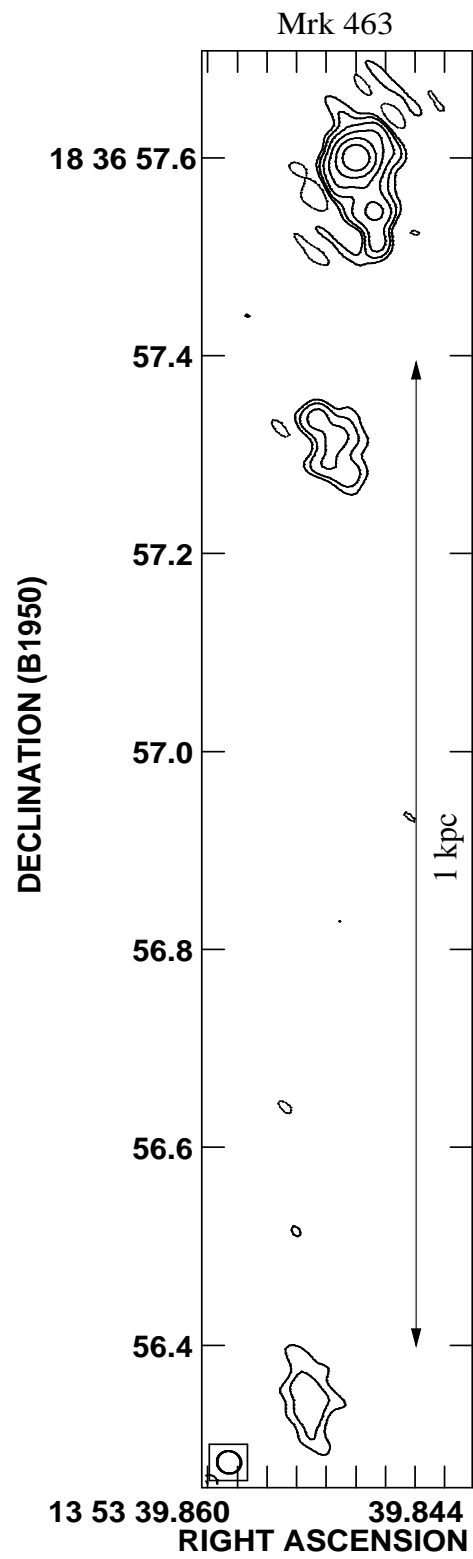


Figure 6

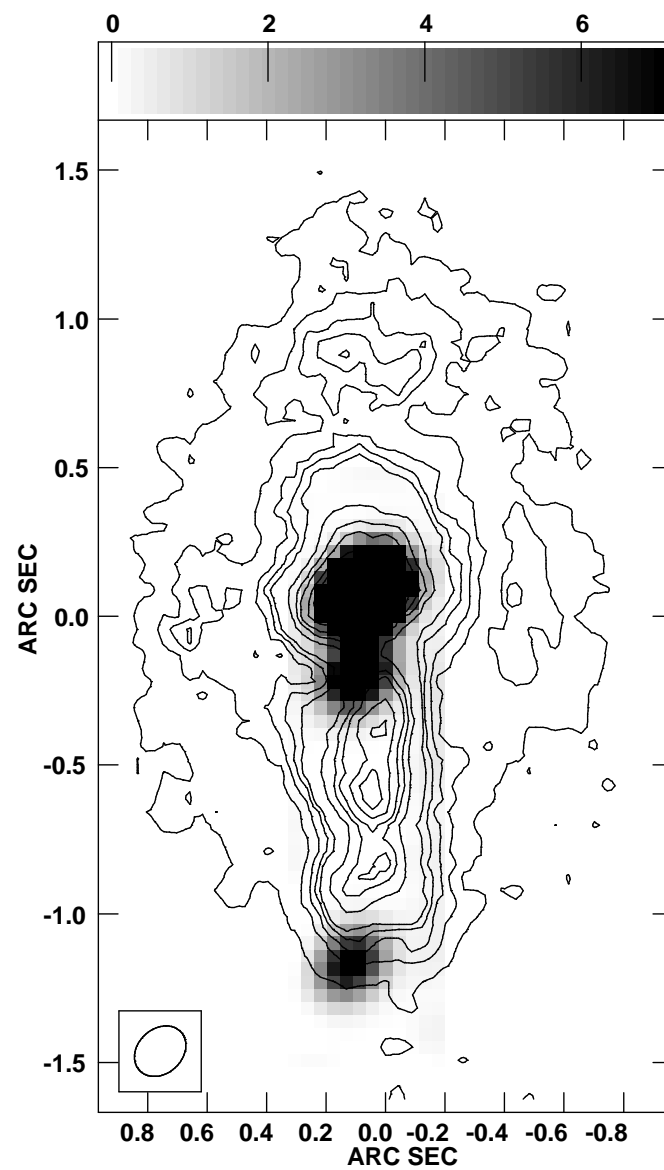


Figure 7